Microporous and Mesoporous Materials 224 (2016) 277–284

Contents lists available at ScienceDirect

Microporous and Mesoporous Materials

journal homepage: www.elsevier.com/locate/micromeso

Hydrothermally stable Zr-doped organosilica membranes for H_2/CO_2 separation

Huating Song [a], Shuaifei Zhao [a, b, *], Jiawei Chen [a], Hong Qi [a, **]

[a] State Key Laboratory of Material-Oriented Chemical Engineering, Membrane Science and Technology Research Center, Nanjing Tech University, Nanjing 210009, Jiangsu, China
[b] Faculty of Science & Engineering, Macquarie University, NSW 2109, Australia

ARTICLE INFO

Article history:
Received 11 November 2015
Received in revised form
31 December 2015
Accepted 2 January 2016
Available online 9 January 2016

Keywords:
Hydrothermal stability
Metal doping
Hybrid silica
Microporous membrane
Gas separation

ABSTRACT

Homogeneous zirconium-doped hybrid organosilica membranes are successfully prepared through the sol–gel route via co-hydrolysis and co-condensation of 1,2-bis(triethoxysilyl)ethane (BTESE) and zirconium n-propoxide (ZrP). Gas permeation measurements and hydrothermal stability tests are carried out for the prepared membranes. Smaller sols are more prone to form a dense structure and thus lead to low gas permeability. Hybrid organosilica membranes with low zirconium content have high hydrogen permeability and H_2/CO_2 selectivity. As zirconium content in the sol increases, membrane structure becomes denser and gas permeability decreases. Excellent hydrothermal stability can be achieved by incorporating Zr into the hybrid silica membranes. This is caused by the improved hydrophobicity due to the presence of hybrid organic-inorganic groups (–Si–CH_2–CH_2–Si–) and the dense, robust membrane structure that formed after zirconium-doping. A ball-and-stick model is proposed based on the characterization data. Our results offer significant insights into understanding the correlations between particles (e.g. size and distribution), structure (e.g. porosity and pore size) and performance (e.g. gas permeability and hydrothermal stability) of organosilica membranes.

1. Introduction

Globally, efficient H_2/CO_2 separation has great significance to both energy security and climate change [1–3]. Hydrogen (H_2) is considered as clean and efficient energy carrier since it has zero greenhouse gas emission during combustion and highest energy content per unit of weight among all the known fuels [4]. H_2 and CO_2 are the major products of water-gas shift (WGS, i.e. $CO + H_2O \rightarrow CO_2 + H_2$) and steam-methane reforming (SMR, i.e. $CH_4 + 2H_2O \rightarrow CO_2 + 4H_2$) reactions. H_2/CO_2 separation is the key step in both hydrogen purification and pre-combustion carbon capture. However, the tiny difference in their kinetic molecular size between H_2 (0.289 nm) and CO_2 (0.33 nm) [5] makes most separation methods very energy intensive.

Membrane separation is one of the most cost-effective and promising technologies for H_2/CO_2 separation. Compared with conventional hydrogen purification methods such as cryogenic distillation and pressure swing adsorption (PSA), membrane separation has the advantages of low energy consumption, low investment cost, ease of operation and possibility for continuous operation [2,4,6]. Various membranes have been extensively investigated for gas separation, including those based on polymer [7], zeolite [8,9], metal [2], metal oxide [10,11], graphene oxide (GO) [12], silica [13,14], metal-organic frameworks (MOFs) [15] and carbon [16,17].

Desirable membranes for efficient H_2/CO_2 separation should have high H_2 permeability and high H_2/CO_2 selectivity. They should also possess excellent mechanical, thermal and chemical stabilities in harsh environments such as high pressure, elevated temperature and steam vapor conditions. However, developing a membrane with all these properties is difficult. For example, palladium membranes are well known for their high H_2 permeance and high H_2/CO_2 selectivity, but suffer from hydrogen embrittlement and contaminant poisoning, resulting in a short lifespan [3,4]. Silica membranes are good candidates for H_2/CO_2 separation due to their

* Corresponding author. Faculty of Science & Engineering, Macquarie University, NSW 2109, Australia. Tel.: +61 2 4960 6127.
** Corresponding author. Tel.: +86 25 83172279.
E-mail addresses: shuaifei.zhao@mymail.unisa.edu.au (S. Zhao), hqi@njtech.edu.cn (H. Qi).

http://dx.doi.org/10.1016/j.micromeso.2016.01.001
1387-1811/

high permeability and selectivity as well as the relatively low cost [13]. Nevertheless, silica membranes exhibit unsatisfactory hydrothermal stability due to the presence of the mobile silanol groups in the membrane matrix [18,19]. Considerable research efforts have been directed to the fabrication of hydrothermally stable silica-based membranes by introducing transition metals or organics [19–25].

Recently, bis(triethoxysilyl)ethane (BTESE), a hydrothermally stable organosilica material with an organic-inorganic structure, has been employed for the fabrication of gas separation membranes [20,26–32]. The presence of hybrid organic-inorganic groups (–Si–CH_2–CH_2–Si–) instead of the original inorganic groups (–Si–O–Si–) in the organosilica membrane matrix increases the hydrophobicity, which prevents water sorption onto or into the material. Thus, the hydrothermal stability of the hybrid organic-inorganic membrane can be effectively improved [20,27,33]. However, the membrane selectivity for H_2/CO_2 is generally not high enough for practical applications [31].

Increasing attention has been paid to zirconia due to its outstanding thermal stability (e.g. melting temperature up to 3043 K) and chemical resistance [34–37]. Zirconium alkoxide has been used to prepare hydrothermally stable silica-zirconia membranes [22]. However, fabrication of defect-free silica-zirconia membranes is still challengeable as zirconium alkoxide is very sensitive to water during the synthesis process of homogeneous sol [35,37]. On the other hand, the membrane pore size is relatively small due to network densification, leading to a low gas permeance [38]. To overcome these issues, recently ten Hove et al. have selected zirconyl nitrate as the precursor to fabricate silica-zirconia membranes [38].

In our previous study [11], pure zirconia membranes with a hydrogen permeance of ~5×10^{-8} mol m^{-2} s^{-1} Pa^{-1} and a H_2/CO_2 permselectivity of ~14 were successfully prepared. In the current study, we fabricated a new hybrid silica-zirconia membrane based on BTESE and zirconium alkoxide via the sol–gel method. The prepared membrane shows excellent hydrothermal stability and high hydrogen permeance due to the special composite network structure. The effect of the zirconium content in the sol on membrane gas separation performance and hydrothermal stability is systematically investigated.

2. Experimental

2.1. Sol preparation

1, 2-bis(triethoxysilyl)ethane (BTESE, a purity of 97%) and zirconium n-propoxide (ZrP, a purity of 70% in n-propanol) from ABCR were used as precursors. 5 mL BTESE and 5 mL absolute ethanol (a purity of 99.7%, Merck) were mixed in a nitrogen glove-box. To obtain a homogeneous BTESE-ethanol solution, the mixture was vigorously stirred with a magnetic stirring apparatus. 0.54 mL nitric acid solution (1 mol/L) was added to the BTESE solution in an ice bath to inhibit the hydrolytic activity of BTESE. Along with continuous stirring, the prepared mixture was kept in a water bath at 60 °C and refluxed for 90 min.

A mixture of ZrP (1.7 mL), n-propanol (20 mL) and acetylacetone (AcAc, 0.1 mL) was introduced into the prepared BTESE sol, followed by adding another 0.54 mL nitric acid solution (1 mol/L). To achieve a uniform mixture, the solution was stirred for 4 min in an ice bath. The Zr-doped hybrid silica (abbreviated as ZS) sol with a molar ratio of 0.14:1 for Zr:Si (abbreviated as ZS14 sol), was synthesized after the reaction at 60 °C for 90 min in a water bath. The ZS14 sol has a molar ratio of 1:0.14:3.27:10.05:2.29:0.04:0.035 for Si:ZrP:C_2H_5OH:n-propanol:H_2O:HNO_3:AcAc. To obtain homogeneous ZS sols with similar size distributions but different zirconium contents, different amounts of ZrP, n-propanol and AcAc were used for preparation of other ZS sols (Table 1). The prepared sols were kept at −20 °C to avoid aggregation prior to further use.

2.2. Characterization of sol and xerogel

The particle size distribution of freshly synthesized ZS sols was measured using a Zetatrac analyzer (NPA152, Microtrac Inc.) on the basis of dynamic light scattering. The hydrodynamic particle diameter was obtained through the detection of light fluctuation caused by Brownian motion of non-spherical hybrid particles. Crystal structure of the unsupported powder calcined at 450 °C was detected by X-ray diffractometer (XRD, MiniFlex 600, Rigaku) with a Cu K_α radiation operated at 40 kV and 15 mA. Fourier transform infrared (FTIR) spectroscopy (NICOLET 8700, Thermo Nicolet Corporation) was used to detect the chemical structure of ZS powders calcined at 450 °C with KBr as the reference. X-ray photoelectron spectroscopy (XPS) measurements were performed on an ESCALAB250xi spectrometer (Thermo Scientific) equipped with a monochromatic Al Kα X-ray source (1486.6 eV). The O1s core-level spectra of ZS powders were deconvoluted by the software package (XPSPEAK41) and relevant details were summarized in Table 2. N_2 and CO_2 (99.99%, Nanjing Special Gases Company) were used to detect the microstructure of ZS powders via the gas adsorption method. N_2 adsorption–desorption isotherms at 77 K and CO_2 adsorption isotherms at 298 K were conducted with a physical adsorption instrument (ASAP 2020, Micromeritics). Prior to the measurements, the samples were degassed under vacuum at 373 K for 12 h.

2.3. Membrane fabrication

To avoid the formation of cracks caused by the capillary force at high Si concentration, the prepared ZS sol was diluted seven times with absolute ethanol before coating. Home-made disc-type γ-Al_2O_3 mesoporous membranes with pore diameter of 3–5 nm were used as the support for Zr-doping. Dip-coating of the ZS sol onto the disc support, was performed with an automatic coating apparatus (Pervatech B. V., the Netherlands) at a velocity of 12 mm s^{-1} under clean room conditions. The calcination was carried out at a rate of 0.5 °C min^{-1} until reaching 450 °C, and was then maintained for 3 h. Next, a cooling procedure was conducted at the same rate of 0.5 °C min^{-1}. The calcination and cooling procedure was conducted under N_2 atmosphere to avoid oxidation. The resultant disc-type samples were the final Zr-doped hybrid silica membranes (referred to as ZS membranes).

2.4. Membrane characterization

2.4.1. Single gas permeation

Single gas permeance of the ZS membrane was measured using a home-made testing apparatus (Fig. 1) [19,39], in which the feed side pressure and the temperature of the membrane module

Table 1
The used quantity of the ingredient in ZS sol preparation (the ingredient of hybrid silica sols was invariable: n(Si): n(C_2H_5OH): n(H_2O): n(HNO_3) = 1: 3.27: 2.29: 0.04).

Zr-doped hybrid silica sols	ZrP/mL	n-propanol/mL	AcAc/mL
ZS14	1.7	20	0.1
ZS25	3	20	0.28
ZS34	4	25	0.55
ZS50	6	30	0.7

Table 2
XPS deconvalution details of O1s peaks of the four ZS membranes.

Sample	[a]BE (eV)	[b]FWHM (eV)	Assignment	Percentage (%)
ZS14	533.11	1.8	Si–O–Si	53.4
	532.02	1.62	Si–O–Zr	34.7
	530.94	1.57	Zr–O–Zr	11.9
ZS25	533.06	1.8	Si–O–Si	45.8
	532.15	1.62	Si–O–Zr	36.7
	530.95	1.57	Zr–O–Zr	17.5
ZS34	533.13	1.8	Si–O–Si	39.4
	531.99	1.62	Si–O–Zr	40.5
	530.86	1.57	Zr–O–Zr	20.1
ZS50	533.28	1.8	Si–O–Si	19.6
	531.88	1.62	Si–O–Zr	54.6
	530.82	1.57	Zr–O–Zr	25.8

[a] BE = Binding energy.
[b] FWHM = Full width at half maximum.

N_2 pressure was maintained at 0.3 MPa with a pressure gauge. The water vapor pressures were controlled between 8 and 100 kPa by adjusting the steam temperatures. After hydrothermal treatment, the membranes were dried for 2 h with a N_2 sweep at the same temperature (i.e. 200 °C). Single gas permeation tests were then performed as described above.

2.4.3. Water contact angle measurement

To evaluate the hydrophobicity/hydrophilicity of the ZS membranes, water contact angle measurements were performed at room temperature by the sessile drop method using a contact angle goniometer (DropMeter A-100P) equipped with a video camera recording system operated using software for drop-shape analysis.

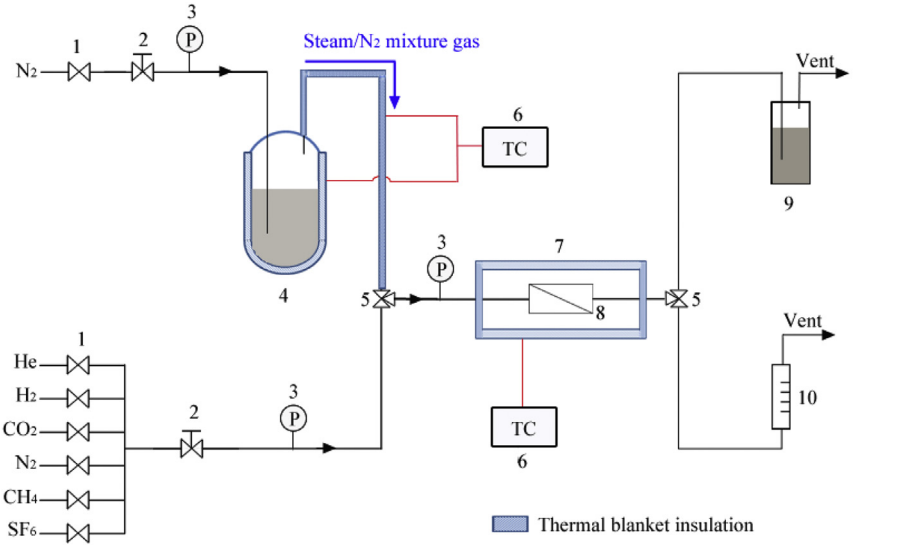

Fig. 1. Experimental apparatus for single gas permeation and hydrothermal stability tests.

were precisely controlled with a pressure controller and a temperature-adjustable furnace, respectively. The membrane was sealed in a stainless steel module with fluoroelastomer O-rings. The permeate side pressure was maintained at the atmospheric pressure. Thus, the transmembrane pressure equaled to the feed side pressure, which was invariably maintained at 0.3 MPa. The test temperature was maintained at 200 °C. The permeation rate was measured with a soap-film flow meter. The membranes were tested with various gases with different kinetic diameters (d_k), including H_2 (d_k = 0.289 nm), CO_2 (d_k = 0.33 nm), CH_4 (d_k = 0.369 nm), O_2 (d_k = 0.345 nm), N_2 (d_k = 0.364 nm), and SF_6 (d_k = 0.55 nm). The gas permselectivity, known as the ideal selectivity, which is equal to the permeance ratio between two gases, then can be obtained.

2.4.2. Hydrothermal stability measurement

In the hydrothermal stability measurement, the ZS membranes were treated at 200 °C in a gas mixture of N_2 and water vapor for at least 8 h with the same apparatus (Fig. 1) described in Section 2.4.1 [39]. First N_2 was humidified and heated in a steam generator. The

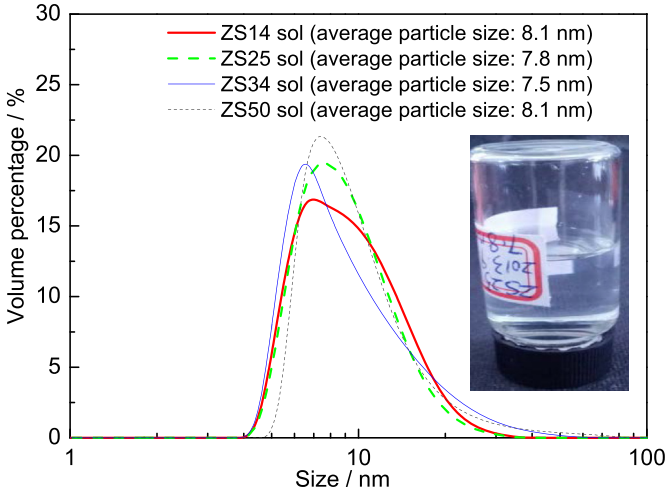

Fig. 2. Particle size distribution of the Zr-doped hybrid silica (ZS) sols.

3. Results and discussion

3.1. Zr-doped silica sol characteristics

Fig. 2 describes the particle size distribution of the Zr-doped silica sols. It can be seen that the four sols have very similar particle size distributions (the dispersity peak is within 7–8 nm) and average particle sizes (~8 nm), particularly for ZS14, ZS25 and ZS50. However, compared with the other three sols, the ZS34 sol shows a slightly lower polydispersity and a slightly smaller average particle size. These small differences may result in a denser membrane with lower gas permeances but high permselectivities, which is confirmed for the ZS 34 sol by the data in Table 3.

The photograph inset into Fig. 2 shows the appearance of the ZS25 sol, which was similar among all sols. It reveals that transparent, homogeneous sols were successfully synthesized under the clean room conditions. For coating to be successful, the particle size of the sol used must fall within a particular range. If the sol particle size is smaller than the pore size of the intermediate layer, then sol will penetrate the intermediate layer, giving the prepared membrane a very low permeability. If the sol particle size is too large, pinholes and defects may occur, giving the prepared membrane a very low selectivity for gases.

Compared with other preparation methods, the sol–gel method is an effective way to fabricate silica membranes with controlled pore sizes [27]. It is known that the sol–gel property has a significant effect on the membrane property [31,40]. For example, the high sintering activity of the relatively small sol particle of ZS34 may lead to a dense structure of the separation layer and thus a low gas permeance. This is confirmed by the following gas permeation data.

3.2. Powder characteristics

Fig. 3 presents the XRD patterns of the ZS powders calcinated at 450 °C. It is obvious that the four XRD patterns are similar and no sharp diffraction peaks of crystalline phase but broad bands can be observed in all the XRD patterns. These results are in agreement with the characteristics of typical microporous materials.

To further understand the chemical composition of the microporous structure, the oxygen atoms and chemical bonds were characterized by XPS and FTIR, respectively. Fig. 4 shows the deconvolution of the XPS O1s peak of the ZS powders with different zirconium contents. It can be seen that the core-level spectra can be decoupled into three peaks with Gaussian contributions corresponding to Si–O–Si (533.10 ± 0.2 eV), Si–O–Zr (532.00 ± 0.2 eV) and Zr–O–Zr (530.90 ± 0.2 eV). The binding energy of Si–O–Si and Zr–O–Zr is slightly higher than pure SiO_2 and ZrO_2 [41]. This suggests more complex chemical states of the oxygen atoms in the ZS powers compared with the pure oxides [42]. These results indicate that the networks of the ZS powders consist of Si–O–Si, Si–O–Zr and Zr–O–Zr structures. In Table 2, it is clear that the content of Si–O–Si decreases when the doped zirconium increases, which is also reflected in Fig. 4. On the contrary, the peaks of Si–O–Zr and Zr–O–Zr become stronger as the zircinium content increases. These results suggest that Si–O–Si bridges decrease but Si–O–Zr and Zr–O–Zr bridges increase in the network structure.

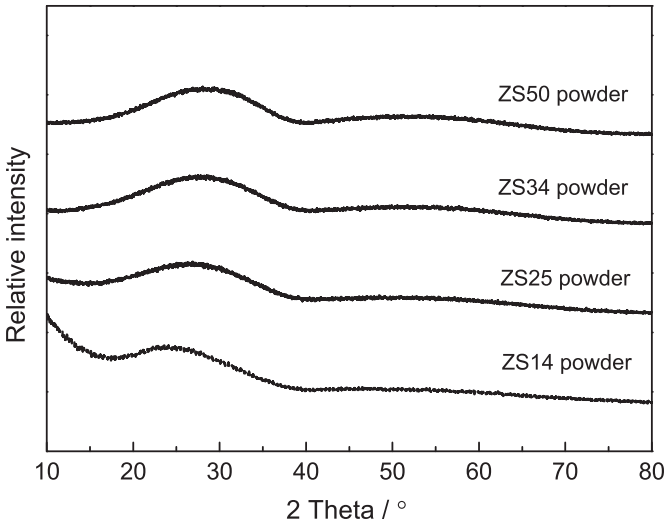

Fig. 3. X-ray diffraction patterns of the Zr-doped hybrid silica (ZS) powders calcined at 450 °C with different zirconium contents.

Fig. 5 reveals FTIR spectra of the ZS powders. The broad bands at approximately 1060 cm^{-1} can be ascribed to asymmetric stretching vibrations of the Si–O–Si groups [43]. The absorption peak at around 1410 cm^{-1} can be assigned to the bending vibrations of CH_2 in the Si–CH_2–CH_2–Si unit [43]. Combining with the results from both XPS and FTIR, we expect that Si–CH_2–CH_2–Si, Si–O–Si, Si–O–Zr and Zr–O–Zr are present in the network structures of the ZS powders.

In this study, N_2 adsorption could not be detected likely due to the relatively dense membrane structure. CO_2 adsorption isotherms of the ZS powders, hybrid SiO_2 powder and ZrO_2 powder are compared in Fig. 6. Obviously, the hybrid silica powder (i.e. organosilica BTESE) shows the highest adsorption capacities, and the pure ZrO_2 powder exhibits the lowest adsorption capacities. The CO_2 adsorption capacities of the Zr-doped silica powders (i.e. ZS powders), decrease as the zirconium content increases. Lower adsorption capacities generally mean denser powder structures. Namely, densification of the ZS powders occurs as the zirconium content increases. Looking carefully, we can also observe that there is no much difference in CO_2 adsorption capacities between the ZS34 powder and the ZS50 powder. This can be explained by the

Table 3
Gas permeance and permselectivity of Zr-doped hybrid silica (ZS) membranes measured at 200 °C.

Membranes	Permeance ($\times 10^{-8}$ mol m^{-2} s^{-1} Pa^{-1})						Permselectivity		
	H_2	CO_2	O_2	N_2	CH_4	SF_6	H_2/CO_2	H_2/N_2	H_2/CH_4
ZS14	7.84	0.66	0.30	0.14	0.10	0.02	12.1	54.9	83.6
ZS25	3.06	0.39	0.13	0.11	0.08	0.03	7.9	29.0	37.8
ZS34	1.15	0.05	0.05	0.02	*	*	23.0	74.0	>1150.0
ZS50	1.03	0.06	0.01	0.03	0.02	0.01	18.5	40.3	50.4
ZrO_2 [11]	4.78	0.32	1.32	1.50	1.29	0.63	14.9	3.2	3.7
Hybrid SiO_2 [31]	46.2	12.4	N/A	4.4	4.0	*	3.7	10.5	11.5

* Permeance is below the detection limit of the equipment.
N/A = relevant data is not available.

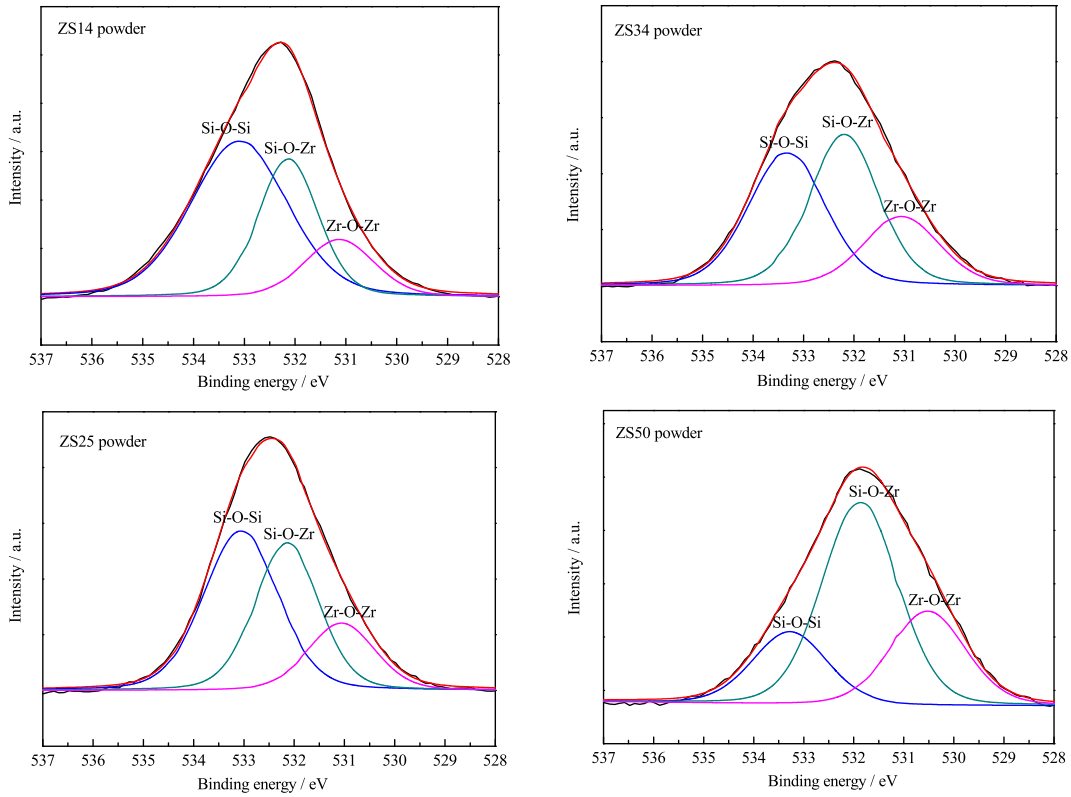

Fig. 4. Deconvolution of the XPS O1s peak of the Zr-doped hybrid silica (ZS) powders calcined at 450 °C with different zirconium contents.

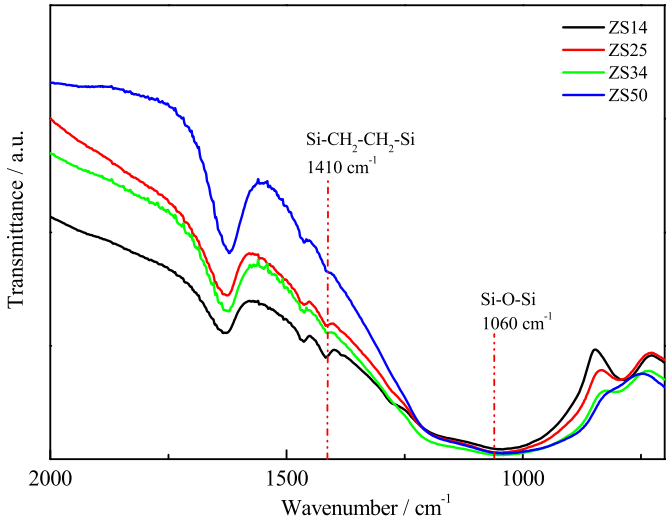

Fig. 5. FTIR spectra of the Zr-doped hybrid silica (ZS) powders calcined at 450 °C with different zirconium contents.

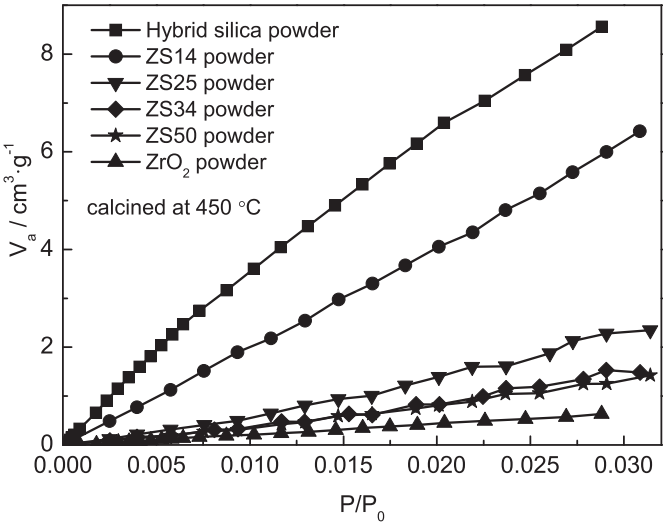

Fig. 6. CO_2 adsorption isotherms of the hybrid silica powder, Zr-doped hybrid silica (ZS) powders, and ZrO_2 powder.

smaller particle size of the ZS34 sol (Fig. 2), which is more prone to result in a denser structure.

The specific surface area was calculated by the Dubinin method modified by Kaganer [33] based on CO_2 uptake data. The results were 120 $m^2\ g^{-1}$ for the hybrid silica powder; 105, 46.8, 27.7 and 25.8 $m^2\ g^{-1}$ for the four ZS powders, respectively; and 13.8 $m^2\ g^{-1}$ for the ZrO_2 powder. These results are in good agreement with the CO_2 adsorption isotherm data (Fig. 6), suggesting that the powder becomes less porous (i.e., denser) from the hybrid silica to the ZS powder to the ZrO_2 powder. It can be summarized that the extent of densification follows the order of: hybrid silica < ZS14 < ZS25 < ZS34 < ZS50 < pure ZrO_2. This offers significant insights into the pore structure of the prepared membranes.

3.3. Gas separation performance of ZS membranes

The single gas (including H_2, CO_2, CH_4, O_2, N_2 and SF_6) permeation results of the ZS membranes are shown in Table 3. The single gas permeance of the ZS membranes decreases as the molecular

kinetic diameter increases, which is due to the molecular sieving effect [44]. The H_2 permeance of the ZS14 membrane reaches 7.84×10^{-8} mol m^{-2} s^{-1} Pa^{-1}, and the ideal selectivity for H_2/CO_2 is 12.1 (Table 3). From Table 3, we can see that the H_2 permeance of the four ZS membranes decreases as the zirconium content rises. This change trend is also applied to other gases with relatively small molecular sizes, such as CO_2, O_2 and N_2. It suggests that the permeation mechanisms of these small gas molecules through the ZS membranes may be the same or similar. The data also agree well with the gas adsorption results (Fig. 6), indicating that a low zirconium content is preferable for a porous structure that will improve gas permeability.

Table 3 shows that the hybrid silica membrane derived from BTESE has the highest gas permeabilities. For example, the permeabilities for H_2 and CO_2 are one order of magnitude higher than those of other membranes. However, the hybrid silica membrane has a lowest H_2/CO_2 selectivity (Table 3). This can be attributed to the relatively open microporous structure of the material [26]. Table 3 also indicates that SF_6 permeance of the ZS34 membrane is below the detection limit of the gas flow meter. This is caused by the small particle size of the ZS34 sol and the resultant densification of the network structure as discussed above. The dense structure of the ZS34 membrane leads to the highest gas selectivities as shown in Table 3. The high gas permeabilities of the hybrid silica membrane and the relatively low gas permeabilities of the ZS membranes are contributed to their special network structures.

Based on all the characterization results above, the difference in the network structure between the hybrid silica membrane and the Zr-doped hybrid silica membrane is schematically illustrated with the ball-and-stick model in Fig. 7. The hybrid silica membrane has relatively large intra-particle pores and loose networks when compared with the Zr-doped hybrid silica membranes. In metallic (e.g. Zr) doping, metal atoms are introduced into the silica networks. As a result, the larger Zr atoms replace the smaller Si atoms in the inherent network structure, leading to a less porous structure. Therefore, the Zr-doped hybrid silica membranes have much lower gas permeabilities than the hybrid silica membrane, and the gas permeabilities decrease with the increase of the Zr content in the membranes (Table 3). Although, incorporating Zr into the hybrid silica networks reduces the membrane intra-pore size and thus the gas permeabilities, it may also increase the hydrothermal stability of the membrane. This is confirmed by the following results.

3.4. Hydrothermal stability evaluation

Fig. 8 shows the changes in gas permeance and permselectivity of the four Zr-doped hybrid silica membranes under various water vapor partial pressures. For the ZS14 membrane, H_2 permeance does not obviously decrease, while CO_2 permeance slightly drops in the first 24 h where the water vapor partial pressures are relatively low (8 or 16 kPa). With further increasing the water vapor partial pressure, H_2 permeance slightly reduces, while CO_2 permeance obviously drops. As a result, H_2/CO_2 permselectivity increases as the water vapor partial pressure rises. This indicates that the ZS14 membrane has excellent hydrothermal stability.

For the other three ZS membranes, the gas permeances clearly falls in the first 8 h under low water vapor partial pressure (8 kPa), but becomes relatively stable upon further increases in water vapor partial pressure. This phenomenon is similar with that reported by Fotou et al. [18] in silica-alumina catalysts.

From Fig. 8, it can also be seen that the CO_2 permeances of the ZS34 and ZS50 membranes are very low, even below the detection limit of the equipment. This is mainly caused by the dense network structures of these membranes. The ZS50 membrane has a dense network structure because of its high Zr content. The structure of the ZS34 membrane is dense mainly due to the smaller particle size of the ZS34 sol (Fig. 2) that is more likely to cause a dense structure. After steam exposure, it is observed that the color of the ZS membranes changes from white to yellow brown as shown in Fig. 9.

In the current study, high hydrothermal stabilities of the ZS membranes can be explained by two reasons. First, the hybrid organic-inorganic groups (–Si–CH_2–CH_2–Si–) in the composite material make the derived ZS membranes less hydrophilic, which helps prevent water penetrating into the membrane structure [20]. The measured water contact angles of the ZS membranes with increasing zirconium content are 77.3°, 74.2°, 73.5° and 69.7°, respectively. Compared with typical pure silica membranes (water contact angle: ~50°) [45], our ZS membranes are less hydrophilic. The pictures of water drops on the ZS membranes are shown in Fig. 10. The water contact angles decrease with the rise in zirconium content, which can be attributed to the replacement of organic groups by inorganic groups (Zr–O–Zr) when the zirconium content in the ZS membranes increases. This is confirmed by the FTIR data (Fig. 5). The absorption peaks of Si–CH_2–CH_2–Si become increasingly weaker as the zirconium content increases.

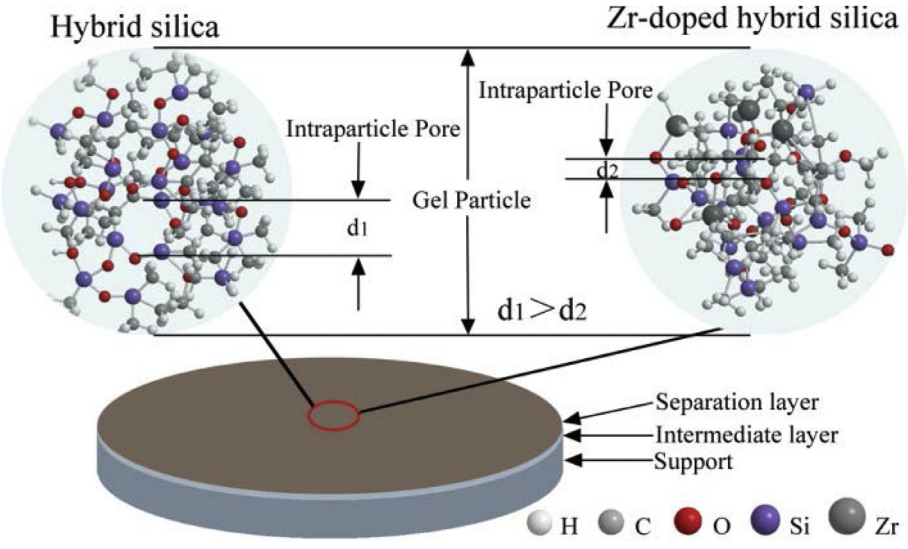

Fig. 7. Schematic comparison of the two types of silica-based membrane.

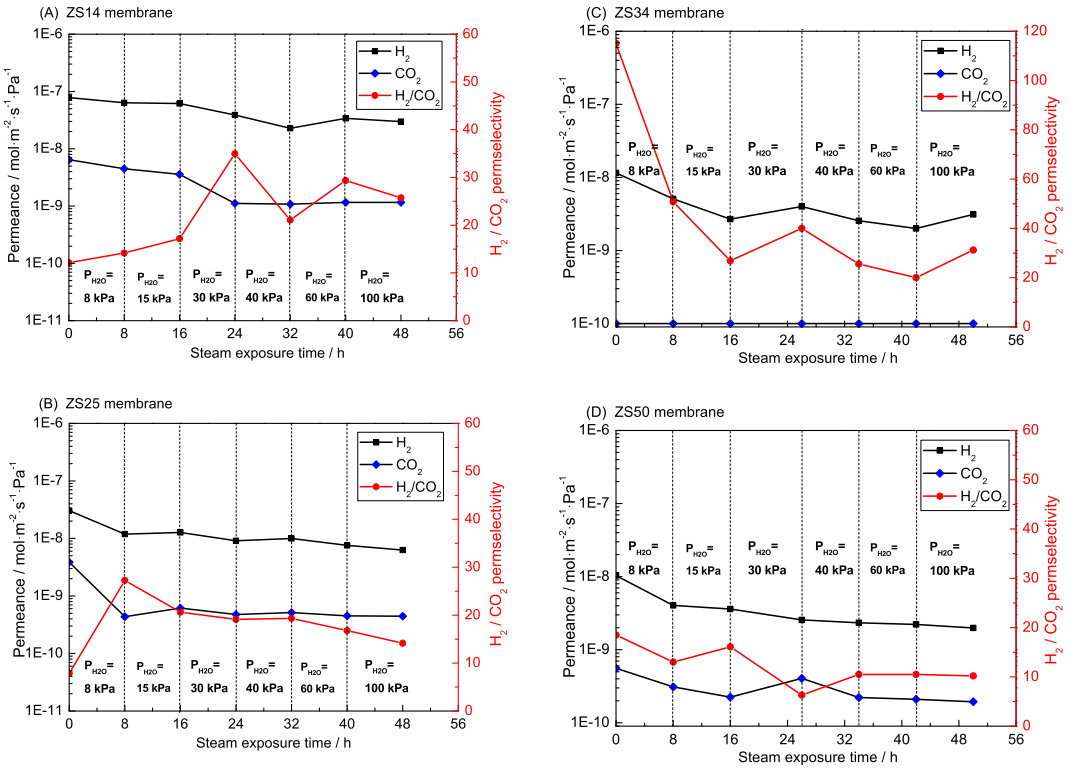

Fig. 8. Gas permeance and permselectivity changes of the four Zr-doped hybrid silica (ZS) membranes under various water vapor partial pressures.

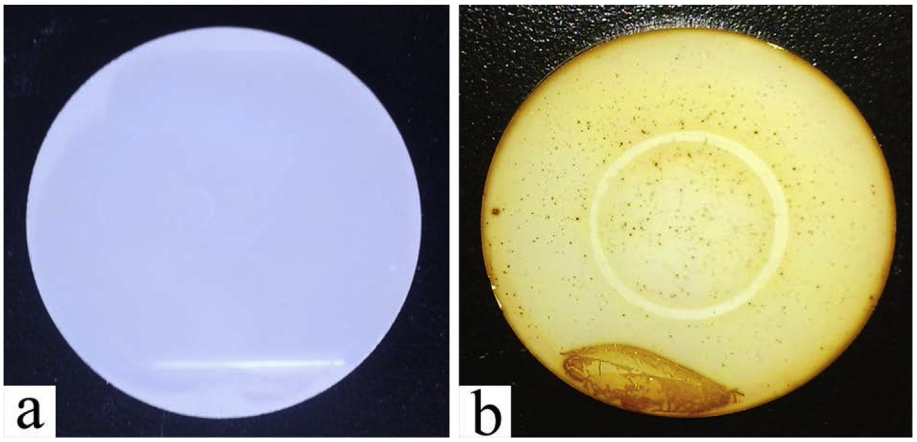

Fig. 9. Photographs of the Zr-doped hybrid silica (ZS) membranes before (a) and after (b) a hydrothermal stability test.

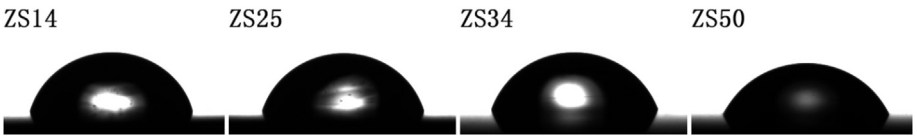

Fig. 10. Pictures of water drops on the four ZS membranes in the water contact angle measurement.

Second, the incorporation of Zr ions into the silica matrix results in more stable architectures [22] and a denser structure which was proven by its CO_2 adsorption (Fig. 6). Here, the Zr is considered to be a network former rather than a network modifier, resulting in a robust structure under thermal and hydrothermal conditions [18].

4. Conclusions

We have successfully prepared homogenous Zr-doped hybrid organosilica membranes using the sol–gel method. Gas permeation measurements and hydrothermal stability tests are carried out for the prepared membranes. It is shown that the particle size of

the sol has an important role in formation of the network structure of the membrane. Smaller sols are more prone to forming a dense structure and thus having low gas permeability. The hybrid organosilica membrane with low zirconium content shows high hydrogen permeability and high H_2/CO_2 selectivity. As the zirconium content in the sol increases, the membrane structure becomes denser and the gas permeability decreases. Excellent hydrothermal stability can be achieved by incorporating zirconium into the hybrid silica membranes. This is mainly caused by the improved membrane hydrophobicity due to the presence of the hybrid organic-inorganic groups ($-Si-CH_2-CH_2-Si-$) and the formed dense and robust structure of the membrane after Zr-doping. We also propose a ball-and-stick model based on the characterization data. The results of this study offer significant insights into understanding the relationships between the membrane material (e.g. particle size), structure (e.g. porosity and pore size) and performance (e.g. gas permeability and hydrothermal stability).

Acknowledgments

This work is supported by the National Natural Science Foundation of China (21276123, 21490581), the National High Technology Research and Development Program of China (2012AA03A606) and the “Summit of the Six Top Talents” Program of Jiangsu Province. We also gratefully acknowledge the financial support from CSIRO's Energy Flagship.

References

[1] A. Brunetti, F. Scura, G. Barbieri, E. Drioli, J. Membr. Sci. 359 (2010) 115–125.
[2] N.W. Ockwig, T.M. Nenoff, Chem. Rev. 107 (2007) 4078–4110.
[3] C.A. Scholes, K.H. Smith, S.E. Kentish, G.W. Stevens, Int. J. Greenh. Gas. Con. 4 (2010) 739–755.
[4] S. Adhikari, S. Fernando, Ind. Eng. Chem. Res. 45 (2006) 875–881.
[5] D.M. D'Alessandro, B. Smit, J.R. Long, Angew. Chem. Int. Ed. 49 (2010) 6058–6082.
[6] P. Bernardo, E. Drioli, G. Golemme, Ind. Eng. Chem. Res. 48 (2009) 4638–4663.
[7] K. Tanaka, M.N. Islam, M. Kido, H. Kita, K. Okamoto, Polymer 47 (2006) 4370–4377.
[8] X.H. Gu, Z. Tang, J.H. Dong, Microporous Mesoporous Mater 111 (2008) 441–448.
[9] S.J. Kim, S.W. Yang, G.K. Reddy, P. Smirniotis, J.H. Dong, Energy Fuels 27 (2013) 4471–4480.
[10] C.C. Coterillo, T. Yokoo, T. Yoshioka, T. Tsuru, M. Asaeda, Sep. Sci. Technol. 46 (2011) 1224–1230.
[11] L. Li, H. Qi, Chin. J. Chem. Eng. 23 (2015) 1300–1306.
[12] H. Li, Z. Song, X. Zhang, Y. Huang, S. Li, Y. Mao, H.J. Ploehn, Y. Bao, M. Yu, Science 342 (2013) 95–98.
[13] R.M. de Vos, Science 279 (1998) 1710–1711.
[14] R.M. de Vos, W.F. Maier, H. Verweij, J. Membr. Sci. 158 (1999) 277–288.
[15] Y. Peng, Y. Li, Y. Ban, H. Jin, W. Jiao, X. Liu, W. Yang, Science 346 (2014) 1356–1359.
[16] J.A. Lie, M.B. Hägg, Carbon 43 (2005) 2600–2607.
[17] M.B. Shiflett, H.C. Foley, J. Membr. Sci. 179 (2000) 275–282.
[18] G.P. Fotou, Y.S. Lin, S.E. Pratsinis, J. Mater. Sci. 30 (1995) 2803–2808.
[19] V. Boffa, D.H.A. Blank, J.E. ten Elshof, J. Membr. Sci. 319 (2008) 256–263.
[20] H.L. Castricum, A. Sah, R. Kreiter, D.H.A. Blank, J.F. Vente, J.E. ten Elshof, Chem. Commun. (2008) 1103–1105.
[21] M.C. Duke, J.C.D. da Costa, D.D. Do, P.G. Gray, G.Q. Lu, Adv. Funct. Mater 16 (2006) 1215–1220.
[22] K. Yoshida, Y. Hirano, H. Fujii, T. Tsuru, M. Asaeda, J. Chem. Eng. Jpn. 34 (2001) 523–530.
[23] R. Igi, T. Yoshioka, Y.H. Ikuhara, Y. Iwamoto, T. Tsuru, J. Am. Ceram. Soc. 91 (2008) 2975–2981.
[24] H.L. Castricum, A. Sah, R. Kreiter, D.H.A. Blank, J.F. Vente, J.E. ten Elshof, J. Mater. Chem. 18 (2008) 2150–2158.
[25] V. Boffa, J.E. ten Elshof, R. Garcia, D.H.A. Blank, Microporous Mesoporous Mater 118 (2009) 202–209.
[26] K.S. Chang, T. Yoshioka, M. Kanezashi, T. Tsuru, K.L. Tung, Chem. Commun. 46 (2010) 9140–9142.
[27] M. Kanezashi, K. Yada, T. Yoshioka, T. Tsuru, J. Am. Chem. Soc. 131 (2009) 414–415.
[28] M. Kanezashi, K. Yada, T. Yoshioka, T. Tsuru, J. Membr. Sci. 348 (2010) 310–318.
[29] X. Ren, K. Nishimoto, M. Kanezashi, H. Nagasawa, T. Yoshioka, T. Tsuru, Ind. Eng. Chem. Res. 53 (2014) 6113–6120.
[30] R. Xu, S.M. Ibrahim, M. Kanezashi, T. Yoshioka, K. Ito, J. Ohshita, T. Tsuru, ACS Appl. Mater. Inter. 6 (2014) 9357–9364.
[31] H.F. Qureshi, A. Nijmeijer, L. Winnubst, J. Membr. Sci. 446 (2013) 19–25.
[32] H.L. Castricum, G.G. Paradis, M.C. Mittelmeijer-Hazeleger, W. Bras, G. Eeckhaut, J.F. Vente, G. Rothenberg, J.E. ten Elshof, Microporous Mesoporous Mater. 185 (2014) 224–234.
[33] H.L. Castricum, G.G. Paradis, M.C. Mittelmeijer-Hazeleger, R. Kreiter, J.F. Vente, J.E. ten Elshof, Adv. Funct. Mater. 21 (2011) 2319–2329.
[34] Y. Gu, K. Kusakabe, S. Morooka, Sep. Purif. Technol. 24 (2001) 489–495.
[35] J.C.S. Wu, L.C. Cheng, J. Membr. Sci. 167 (2000) 253–261.
[36] J. Fan, H. Ohya, T. Suga, H. Ohashi, K. Yamashita, S. Tsuchiya, M. Aihara, T. Takeuchi, Y. Negishi, J. Membr. Sci. 170 (2000) 113–125.
[37] G. Zhu, Q. Jiang, H. Qi, N. Xu, Chin. J. Chem. Eng. 23 (2014) 31–41.
[38] M. ten Hove, A. Nijmeijer, L. Winnubst, Sep. Purif. Technol. 147 (2015) 372–378.
[39] H. Qi, Chin. J. Chem. Eng. 19 (2011) 404–409.
[40] T. Tsuru, J. Sol-Gel Sci. Technol. 46 (2008) 349–361.
[41] M.J. Guittet, J.P. Crocombette, M. Gautier-Soyer, Phys. Rev. B 63 (2001) 125117.
[42] R.L. Opila, G.D. Wilk, M.A. Alam, R.B. van Dover, B.W. Busch, Appl. Phys. Lett. 81 (2002) 1788–1790.
[43] P.H.T. Ngamou, J.P. Overbeek, R. Kreiter, H.M. van Veen, J.F. Vente, I.M. Wienk, P.F. Cuperus, M. Creatore, J. Mater. Chem. A 1 (2013) 5567–5576.
[44] H.R. Lee, M. Kanezashi, Y. Shimomura, T. Yoshioka, T. Tsuru, AlChE J. 57 (2011) 2755–2765.
[45] B. Bettens, S. Dekeyzer, B. Van der Bruggen, J. Degrève, C. Vandecasteele, J. Phys. Chem. B 109 (2005) 5216–5222.